

Current partition at topological zero-line intersections

Zhenhua Qiao,¹ Jeil Jung,¹ Chungwei Lin,¹ Allan H. MacDonald,¹ and Qian Niu^{1,2}

¹*Department of Physics, The University of Texas at Austin, Austin, Texas 78712, USA*

²*International Center for Quantum Materials, Peking University, Beijing 100871, China*

(Dated: February 27, 2013)

An intersection between one-dimensional chiral acts as a topological current splitter. We find that the splitting of a chiral zero-line mode obeys very simple, yet highly counterintuitive, partition laws which relate current paths to the geometry of the intersection. Our results have far reaching implications for device proposals based on chiral zero-line transport in the design of electron beam splitters and interferometers, and for understanding transport properties in systems where multiple topological domains lead to a statistical network of chiral channels.

A massive chiral two-dimensional electron gas (C2DEG) has a valley Hall conductivity that has the same sign as its mass. The valley Hall effect leads to conducting edge states and also, when the mass parameter varies spatially, to conducting states localized along mass zero-lines.¹⁻³ Provided that inter-valley scattering is weak, zero-line state properties are closely analogous¹⁻³ to edge state properties of quantum spin-Hall insulators and include both chiral propagation and suppressed backscattering.¹ Metallic zero-line modes (ZLMs), or topological 1D kink states, provide a two dimensional realization of Dirac zero energy modes,^{4,5} and their existence has been proposed in a wide variety of systems including graphene mono and bilayers,^{1-3,6-8} topological insulators with lattice dislocations,⁹ boron nitride crystals with grain boundaries,¹⁰ superfluid ³He,¹¹ and photonic crystals.^{12,13} In the present Letter we examine current partition properties at zero-lines intersections,^{1,3} which are expected to be ubiquitous in systems in which the mass term results from a disorder potential or from spontaneous symmetry breaking.

ZLMs in C2DEGs are centered on zero-lines of the mass^{1-3,6,7}, *i.e.* on lines along which the mass changes sign as illustrated in Figure 1a. A mass term leading to a valley Hall effect^{14,15} can be produced by a sublattice staggered external potential in single layer graphene,^{6,7} and more practically by a gate controlled interlayer potential difference in Bernal bilayer and ABC stacked multilayer graphene.^{1-3,8} Mass terms can also be generated by spin-orbit coupling¹⁶⁻¹⁸ and by electron-electron interactions.¹⁹⁻²¹ In this last case ZLMs²² appear naturally at domain walls separating regions with different local anomalous, spin, or valley Hall conductivities.

Chiral propagation implies that ZLMs can travel only in the direction which places negative masses either on their left, or depending on valley, on their right. It follows, as illustrated in Figure 1c, that there is no forward propagation at a zero-lines intersection; a propagating mode is split between a portion that turns clockwise and a portion that turns counterclockwise. These unusual transport properties are potentially valuable for new types of electronic devices. We have therefore carried out quantum transport calculations for an explicit model of intersecting ZLMs in order to discover rules for current

partitioning at such a ZLM splitter. The system we study is a π -band tight-binding model for single-layer graphene with a position-dependent sublattice-staggered potential constructed to form intersecting zero lines which enable propagation to four ZLMs labeled left (L), right (R), up (U) and down (D) in Figure 1b. For simplicity, we consider the case where the U and D ZLMs are fixed along the vertical direction, and we define the angles between R and D ZLMs to be α and between L and U ZLMs to be β . The blue and orange lines in Figure 1b indicate the allowed chiral propagation paths.

The numerical results reported on below are for a π -orbital tight-binding Hamiltonian with nearest neighbor hopping and a sublattice-staggered potential: $H = -t \sum_{\langle ij \rangle} c_i^\dagger c_j + U_A \sum_{i,A} c_i^\dagger c_i + U_B \sum_{i,B} c_i^\dagger c_i$. Here c_i^\dagger (c_i) is a creation (annihilation) operator for an electron at site i , and $t = 2.6$ eV is the nearest neighbor hopping amplitude. For a sublattice staggered potential the A and B sublattice energies are opposite, *i.e.* $U_A = -U_B = \lambda U_0$, where U_0 measures the potential strength and $\lambda = \pm$ determines the sign of the valley Hall effect in each quadrant. In all our simulations, the potential amplitude was chosen to be $U_0/t = 0.05$. The ZLMs appear confined along zero-lines where the mass becomes zero and the resulting wave-function tails spread into the bulk with a depth proportional to the inverse of the mass^{1,3}.

Although our study has been carried out in single layer graphene for computational convenience, we expect that similar conclusions apply to ZLMs in other systems, and in particular in bilayer graphene where the spatially patterned mass term can in principle be generated externally using gates. Our transport calculations are based on the Landauer-Büttiker formalism²³ and recursively constructed Green functions.^{24,25} The conductance from lead q to lead p is numerically evaluated from $G_{pq} = (e^2/h) \text{Tr}[\Gamma_p G^r \Gamma_q G^a]$, where e is the electron charge, h is the Planck's constant, $G^{r,a}$ are the retarded and advanced Green's functions,²³ and Γ_p is a linewidth function describing the coupling between lead p and the central region. The propagation of ZLMs, or kink states, incoming from lead p is effectively illustrated by plotting a map of its contribution to the local density of states (LDOS) at an energy ε in the gap: $\rho_p(\mathbf{r}, \varepsilon) = 1/2\pi [G^r \Gamma_p G^a]_{\mathbf{r}\mathbf{r}}$. Here \mathbf{r} is the real space co-

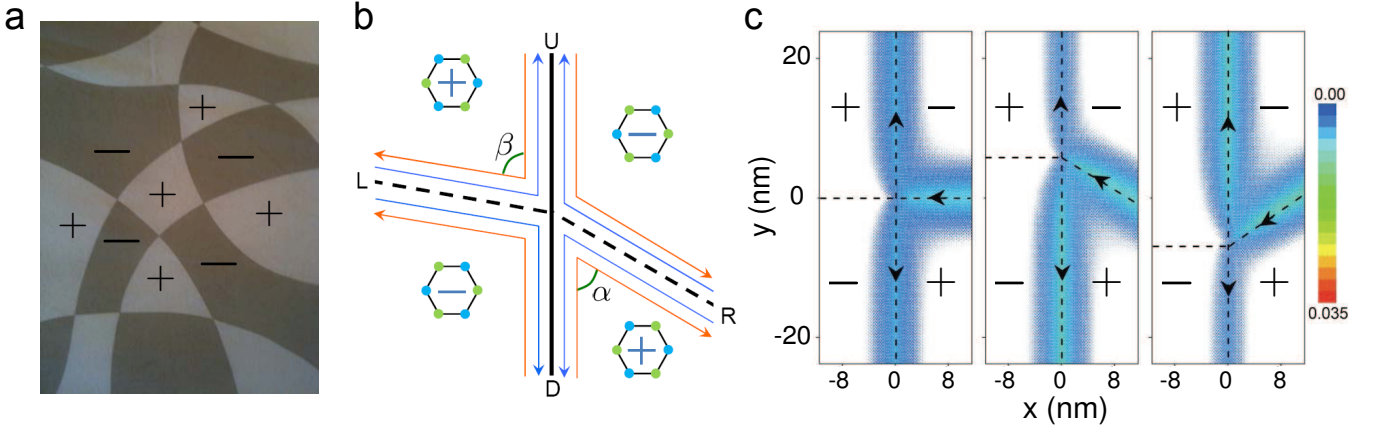


FIG. 1: **Current partition at zero-line intersections:** **a.** Staggered sub lattice-potential, and hence valley Hall conductivity, spatial distribution pattern which defines the zero-line paths. Blue dots indicate positive site energies and green dots negative site energies. **b.** Schematic of four-terminal graphene samples with different staggered potential distributions. The Left (L), right (R), up (U), and down (D) leads are extend indefinitely from the plotted central scattering region. The U and D ZLMs are fixed along the vertical direction and the angles α and β specify the R and L ZLM directions. The solid and dashed lines in black denote zero lines. The blue and orange lines represent allowed chiral propagation paths. **c.** ZLM LDOS distribution for modes incident from lead R for $\alpha = 90^\circ, 60^\circ, 120^\circ$ at fixed $\beta = 90^\circ$.

ordinate.

The central scattering region in our calculations is rectangular with size $n_x = 94$ and $n_y = 432$ as explained fully in the Supplementary Information. The valley label of a state is of course not a good quantum number for ZLMs and valleys are most strongly mixed when their wave vector projections in the propagation direction are identical. For energies inside the gap this coincidence happens only for propagation in the armchair direction^{1,2,6,10}. However, numerical calculations have shown a remarkable absence of back-scattering at sharp turns in the zero-line or at the encounter of a ZLM splitter¹ except in a narrow energy range very close to the avoided crossing gap centered on $\varepsilon/t = 0.00$ between modes with opposite propagation directions. For the results shown below we have chosen $\varepsilon/t = 0.01$ to avoid this energy range; the chirality of the ZLM modes is then very well defined.

In a four terminal ZLM splitter device [see Figures 1b], there are in total twelve distinct inter-terminal conductance values. The number of independent conductances is reduced to six in time-reversal symmetric systems since $G_{pq} = G_{qp}$. For chiral transport forward scattering and back scattering are absent at a ZLM intersection, reducing the number of independent parameters further. The current conservation then implies that $G_{pr} + G_{qr} = G_0 = e^2/h$ for any value of r and p, q the labels of the two neighboring leads. It follows that

$$G_{LU} = G_{RD} \quad \& \quad G_{RU} = G_{LD}, \quad (1)$$

and that $G_{RU} + G_{RD} = e^2/h$, leaving only one independent parameter for the entire four terminal systems. In a ZLM splitter with zero backscattering and perfect chiral current filtering transport is completely characterized by specifying how incoming current at an intersection is

partitioned between clockwise and counterclockwise rotation outgoing directions. The partition law must be the same for all incoming channels. In the following, we focus on the conductances G_{UR} and G_{DR} corresponding to the currents incoming from lead R. The above relations were numerically verified for a ZLM current splitter with $\alpha = \beta = 90^\circ$ in Ref. [1] and we have now numerically verified that they are true for arbitrary values of the lead angles α and β . (See the Supplementary Information for further details.)

For a ZLM splitter with a fixed vertical pair of leads U and D and rotatable R and L leads as shown in Figure 1b, we have numerically discovered a rather simple law which describes the dependence of the current partition on the angles α and β with surprising accuracy: (See Figure 2 for a summary of the data which supports this law and the Supplementary Information for further details.)

$$\begin{aligned} G_{UR} &= \frac{G_0}{2} [1 - \sin(\alpha + \beta)], \\ G_{DR} &= \frac{G_0}{2} [1 + \sin(\alpha + \beta)], \end{aligned} \quad (2)$$

for $90^\circ \leq \alpha + \beta \leq 270^\circ$. Outside of this angle range the current follows the path with the larger rotation angle: $G_{DR} = G_{UL} = G_0$ and $G_{UR} = G_{DL} = 0$ when $0^\circ < \alpha + \beta < 90^\circ$, or $G_{UR} = G_{DL} = G_0$ and $G_{DR} = G_{UL} = 0$ when $270^\circ < \alpha + \beta < 360^\circ$. For the special case of $\beta = 90^\circ$ the current partition law simplifies to $G_{UR} = G_0 \sin^2(\alpha/2)$ and $G_{DR} = G_0 \cos^2(\alpha/2)$. And for the special case of $\alpha = \beta$, corresponding to zero lines that are straight at the intersection point and therefore to a mass pattern defined by a smooth external potential, $G_{UR} = G_0 \sin^2(\alpha - 45^\circ)$ and $G_{DR} = G_0 \cos^2(\alpha - 45^\circ)$.

Contrary to intuition, as illustrated in Figure 1c for a current incoming from lead R, the current partition

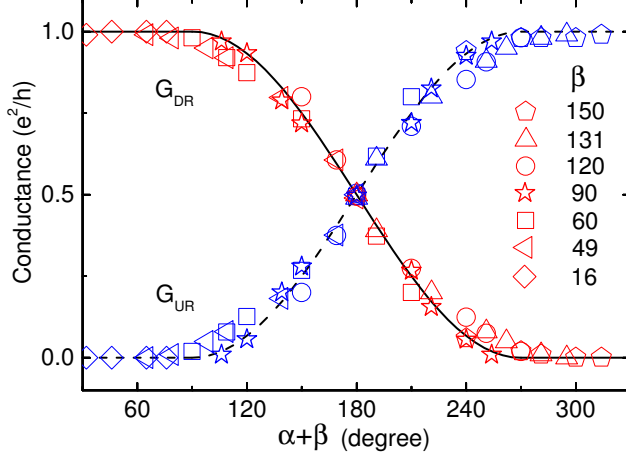


FIG. 2: **Current partition law:** Current as a function of angles α and β for the zero-line intersection defined in Fig. 1c. The current partition follows a simple relation given by Eq. 2 whenever $90^\circ \leq \alpha + \beta \leq 270^\circ$ and completely follows the sharper rotation path outside this range. The solid and dashed lines are the fitting functions defined in Equation (2).

law implies that more current always follows the path requiring a larger rotation angle. This makes sense since this pair of incoming and outgoing modes interact over a longer distance, providing more opportunity for interactions which lead to inter-mode scattering (The zero-line mode decay length is $\sim mv_D/\hbar$ where m is the local mass and v_D is the Dirac point velocity for $m \equiv 0.6$). It is noteworthy that the current partition depends only on the combination $\alpha + \beta$ and indeed it is surprising that the angle β , which specifies the orientation of a lead that does not carry any current, influences the partition law. This law evidently results, however, from the interference between ZLMs close to the ZLM intersection point, allowing inactive leads to play a role in the scattering. Note that the completely unbalanced current partition favored by a very small value of α (a sharp turn from R to D) is mitigated if β (the L to U turn angle) is larger than 90° .

We emphasize we have not derived the form which fits our current partition numerical results analytically and it is likely only approximate. It applies accurately only at energies close to the middle of the bulk energy gaps. The expression can be rationalized by the following argument. Let us consider a ZLM splitter, where the chiral current filtering rule restricts current incoming from R or L to scatter into the U and D leads. By denoting the asymptotic amplitudes of the ZLM at the leads as A_R , A_L , A_U , and A_D , current conservation implies that

$$\begin{bmatrix} A_U \\ A_D \end{bmatrix} = \begin{bmatrix} \cos(\tau)e^{iu} & -\sin(\tau)e^{-iv} \\ \sin(\tau)e^{iv} & \cos(\tau)e^{-iu} \end{bmatrix} \begin{bmatrix} A_L \\ A_R \end{bmatrix}. \quad (3)$$

Equation (3) relates the amplitudes of incoming and outgoing waves via a general SU(2) unitary transformation matrix with parameters u , v , and τ . When we set A_L to be zero, then for any A_R , $|A_U|^2 = |A_R|^2 \sin^2 \tau$,

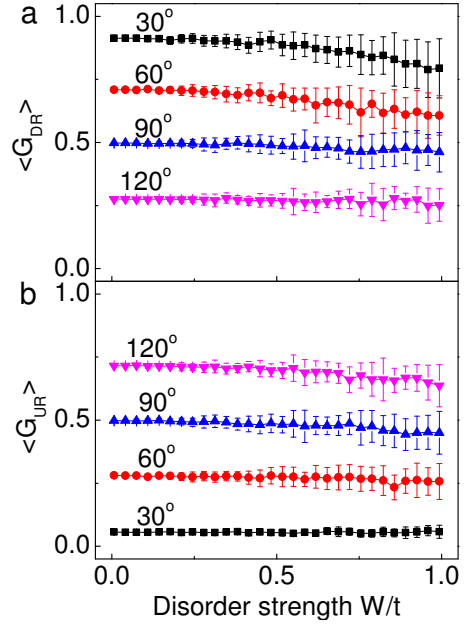


FIG. 3: **Influence of disorder on the current partition law:** Averaged conductances $\langle G_{DR} \rangle$ (in panel a) and $\langle G_{UR} \rangle$ (in panel b) from lead R to leads D and U as a function of disorder strength W at fixed $\beta = 90^\circ$. Four representative angles of incidence $\alpha = 30^\circ$, 60° , 90° , and 120° are considered. Over 50 samples are collected at each point. The error bar is used to indicate the strength of fluctuations as a function of disorder realization.

and $|A_D|^2 = |A_R|^2 \cos^2 \tau$. The scattering phases u and v are irrelevant for the scattering probability and will henceforth be dropped. The conductances from R can thus be written as $G_{UR} = G_0 \sin^2 \tau(\alpha, \beta)$ and $G_{DR} = G_0 \cos^2 \tau(\alpha, \beta)$, where $G_0 = e^2/h$. Equipartition for $(\alpha, \beta) = (\alpha, 180^\circ - \alpha)$ implies that $\tau(\alpha, 180^\circ - \alpha) = 45^\circ$. For the current coming from R into D lead, we get from symmetry considerations the relation $G_{DR}(\alpha, \beta) = G_{DR}(\beta, \alpha)$. If we assume that τ is a smooth function of α and β and additionally require that the conductances are invariant under $(\alpha, \beta) \rightarrow (\alpha + N \times 360^\circ, \beta + M \times 360^\circ)$ we can conclude that $\tau(\alpha, \beta) = c(\alpha + \beta)/2 - 45^\circ$, where $c = \pm 1$. Then we impose a second condition for the current partition saturation when $\alpha + \beta = 90^\circ$, for instance in the limit when $\beta = 90^\circ$ and $\alpha = 0^\circ$ where R and D ZLMs merge together, that further restricts $c = +1$. This expression reproduces Equation (2) for G_{DR} and G_{UR} , outside the saturation region which occurs for $\alpha + \beta < 90^\circ$ and $\alpha + \beta > 270^\circ$.

Now we examine the robustness of our results in the presence of disorder. Long-range disorder is not effective in producing inter valley scattering¹ so we focus on the potentially more important short-range disorder which we model as a random potential at each lattice site. Specifically we add a term $H_{dis} = \sum_i \omega_i c_i^\dagger c_i$ with ω_i being uniformly distributed in the interval of $[-W/2, +W/2]$, where W characterizes the disorder strength. In our simulations we considered over 50 real-

izations of the random disorder potential for each value of the strength. Figure 3 illustrates our results for the average conductances $\langle G_{UR} \rangle$ and $\langle G_{DR} \rangle$ as a function of disorder strength W . We see that the current partition law remains accurate up to disorder strengths larger than the bulk band gap $\Delta/t = 0.1$. When the disorder strength is further increased, the averaged conductances $\langle G_{UR} \rangle$ and $\langle G_{DR} \rangle$ are slightly reduced and disorder fluctuations grow. For example, when the disorder strength reaches $W/t = 1.0$, 10 times larger than the bulk band gap, the averaged conductances still retain over 80% of their original values. The lost current takes advantage of the intervalley scattering to access the outgoing modes of the L lead or to backscatter in the R lead. All these findings strongly indicate that the current partition law is very robust to disorder, suggesting that ideal zero-line transport properties can be approximated in real devices.

Since there are presently no practical techniques for imposing staggered sublattice potentials in single layer graphene, other closely related systems may ultimately be of greater experimental interest. In Bernal stacked bilayer graphene, for example, a ZLM splitter can be realized by using gates to achieve perpendicular electric fields which vary in sign spatially. Another possibility is 2D honeycomb photonic crystals, in which the Dirac points have been experimentally observed and sublattice staggered potentials can be realized by choosing different diameters for the cylinders which form the structure or by varying the dielectric material used.

In summary, when intervalley scattering can be neglected, transport along the zero lines of a sublattice-staggered potential in graphene is chiral, requiring travel in a direction which keeps positive masses on either the

left or the right, depending on valley. We have used the Landauer-Buttiker formula and recursively constructed Green's functions to examine how chiral currents are partitioned between available outgoing leads at a ZLM intersection. We find that at energies near the middle of the bulk gap our numerical results for the dependence of current on ZLM geometry are accurately described by a simple partition law specified in Eq. (2), and that the influence of disorder on this law is weak. The helicity of ZLM provides a new mechanism for allowing or blocking currents and may find applications in alternative designs for nanoelectronic devices or in enabling electron quantum interferometry²⁶ in a new setting. We have explored, for the first time to our knowledge, the geometry-dependent current partition laws at the intersection of two zero-lines. It will be interesting to extend our present studies to more general parameter spaces and to look for similarities and differences with respect to other systems with chiral 1D transport channels including photonic crystals, quantum anomalous Hall and quantum Hall effect systems, and chiral superconductors.

Acknowledgements.— We are grateful to Wang-Kong Tse, Wang Yao, Jian Li and Yue Yu for useful discussions and P. J. Coulchinsky for his help with figures. This work was financially supported by the Welch Foundation (F-1255 and TBF1473), and by DOE (DE-FG03-02ER45958, Division of Materials Science and Engineering) grant. Additional support was provided by grants NBRPC (2012CB-921300) and NSFC (91121004). The Computer Center of The University of Hong Kong is gratefully acknowledged for high-performance computing assistance [supported in part by a Hong Kong UGC Special Equipment Grant (SEG HKU09)].

-
- ¹ Qiao, Z. H., Jung, J., Niu, Q. & MacDonald, A. H. Electronic highways in bilayer graphene. *Nano Lett.* **11**, 3453-3459 (2011).
 - ² Jung, J., Zhang, F., Qiao, Z. H. & MacDonald, A. H. Valley-Hall kink and edge states in multilayer graphene. *Phys. Rev. B* **84**, 075418 (2011).
 - ³ Martin, I., Blanter, Ya. M. & Morpurgo, A. F. Topological confinement in bilayer graphene. *Phys. Rev. Lett.* **100**, 036804 (2008).
 - ⁴ Jackiw, R. & Rebbi, C. Solitons with fermion number 1/2. *Phys. Rev. D* **13**, 3398 (1976).
 - ⁵ Su, W. P., Schrieffer, J. R. and Heeger, A. Solitons in polyacetylene, *Phys. Rev. Lett.* **42**, 1698 (1979).
 - ⁶ Semenoff, G. W., Semenoff, V. & Zhou, F. Domain walls in gapped graphene. *Phys. Rev. Lett.* **101**, 087204 (2008).
 - ⁷ Yao, W., Yang, S. A. & Niu, Q. Edge states in graphene: from gapped flat-band to gapless chiral modes. *Phys. Rev. Lett.* **102**, 096801 (2009).
 - ⁸ Killi, M., Wu, S. & Paramekanti, A. Band structures of bilayer graphene superlattices. *Phys. Rev. Lett.* **107**, 086801 (2011).
 - ⁹ Ran, Y., Zhang, Y. & Vishwanath, A. One-dimensional topologically protected modes in topological insulators with lattice dislocations. *Nature Phys.* **5**, 298-303 (2009).
 - ¹⁰ Jung, J., Qiao, Z. H., Niu, Q. & MacDonald, A. H. Transport properties of graphene nanoroads in boron nitride sheets. *Nano Lett.* **12**, 2936-2940 (2012).
 - ¹¹ Volovik, G. E. *The Universe in a Helium Droplet* (Oxf. Univ. Press, Oxford, U.K., 2003).
 - ¹² Ochiai, T. & Onoda, M. Photonic analog of graphene model and its extension: Dirac cone, symmetry, and edge states. *Phys. Rev. B* **80**, 155103 (2009).
 - ¹³ Khanikaev, Alexander B., Mousavi, S. Hossein, Tse, Wang-Kong, Kargarian, Mehdi, MacDonald, Allan H., & Shvets, Gennady Photonic topological insulators. *Nature Materials* doi:10.1038/nmat3520.
 - ¹⁴ Xiao, D., Yao, W. & Niu, Q. Valley-contrasting physics in graphene: magnetic moment and topological transport. *Phys. Rev. Lett.* **99**, 236809 (2007).
 - ¹⁵ Li, J., Martin, I., Büttiker, M. & Morpurgo, A. F. Topological origin of subgap conductance in insulating bilayer graphene. *Nature Phys.* **7**, 38 (2011).
 - ¹⁶ Qiao, Z. H., Yang, S. A., Feng, W., Tse, W.-K., Ding, J., Yao, Y., Wang, J. & Niu, Q. Quantum anomalous Hall effect in graphene from Rashba and exchange effects. *Phys. Rev. B* **82**, 161414 (2010).

- ¹⁷ Kane, C. L. & Mele, E. J. Quantum Spin Hall Effect in Graphene. *Phys. Rev. Lett.* **95**, 226801 (2005)
- ¹⁸ Qiao, Z. H., Tse, W.-K., Jiang, H., Yao, Y. & Niu, Q. Two-dimensional topological insulator state and topological phase transition in bilayer graphene. *Phys. Rev. Lett.* **107**, 256801 (2011).
- ¹⁹ Zhang, F., Jung, J., Fiete, G. A., Niu, Q. & MacDonald, A. H. Spontaneous quantum Hall states in chirally stacked few-layer graphene systems. *Phys. Rev. Lett.* **106**, 156801 (2011).
- ²⁰ Jung, J., Zhang, F., MacDonald, A. H. Lattice theory of pseudospin ferromagnetism in bilayer graphene: Competing interaction-induced quantum Hall states. *Phys. Rev. B* **83**, 115408 (2011).
- ²¹ Nandkishore, R. & Levitov, L. Quantum anomalous Hall state in bilayer graphene. *Phys. Rev. B* **82**, 115124 (2010).
- ²² Zhang, F., Jung, J. & MacDonald, A. H. Spontaneous quantum Hall states and novel luttinger liquids in chiral graphene, *Journal of Physics: Conf. Ser.* **334**, 012002 (2011).
- ²³ Datta, S. *Electronic Transport in Mesoscopic Systems* (Camb. Univ. Press, Cambridge, 1995).
- ²⁴ Lopez Sancho, M. P., Lopez Sancho, J. M. & Rubio, J. Quick iterative scheme for the calculation of transfer matrices: application to Mo (100). *J. Phys. F: Met. Phys.* **14** 1205 (1984).
- ²⁵ Wang, J. & Guo, H. Relation between nonequilibrium Green's function and Lippmann-Schwinger formalism in the first-principles quantum transport theory. *Phys. Rev. B* **79**, 045119 (2009).
- ²⁶ Ji, Y., Chung, Y., Sprinzak, D., Heiblum, M., Mahalu, D. & Shtrikman, H. An electronic Mach-Zehnder interferometer. *Nature* **422**, 415-418 (2003).